Available online at www.sciencedirect.com
ScienceDirect
International Journal of Heat and Fluid Flow 28 (2007) 735–752
International Journal of HEAT AND FLUID FLOW
www.elsevier.com/locate/ijhff

Drop impacts onto cold and heated rigid surfaces: Morphological comparisons, disintegration limits and secondary atomization

A.S. Moita, A.L.N. Moreira *

Instituto Superior Técnico, Mechanical Engineering Department, Center for Innovation, Technology and Policy Research, IN+ Av. Rovisco Pais 1049-001, Lisboa Codex, Portugal

Received 8 July 2005; received in revised form 2 May 2006; accepted 21 October 2006
Available online 22 December 2006

Abstract

This paper addresses an experimental study aimed at characterizing the mechanisms of disintegration which occur when individual water and fuel droplets impact onto heated surfaces. The experiments consider the use of a simplified flow configuration and make use of high-speed visualization together with image processing techniques to characterize the morphology of the impact and to quantify the outcome of secondary atomization in terms of droplet size and number.

The results evidence that surface topography, *wettability* and liquid properties combine in a complex way to alter the wetting behaviour of droplets at impact at different surface temperatures. The relative importance of the dynamic vapor pressure associated with the rate of vaporization and surface roughness increases with surface temperature and becomes dominant at the film boiling regime. The analysis is aimed at giving a phenomenological description of droplet disintegration within the various heat transfer regimes.

Keywords: Drop impact; Disintegration mechanisms; Boiling regimes; Nature of the surface; Drop morphology; Secondary droplet characteristics

1. Introduction

The performance and pollutant emissions of IC engines depend on fuel atomization and mixture preparation prior to combustion, which, in turn are affected by the interaction of fuel droplets with interposed surfaces. For instance, in port fuel injection systems, it is a common practice to target the fuel spray onto the back of the inlet valves, so that the high surface temperature (which may be larger than 200 °C) enhances fuel evaporation. However, a significant part of the injected fuel deposits onto surfaces, generating a liquid film which does not have time to vaporize before the intake stroke, leading to the formation of unburned hydrocarbons (HC emissions), particularly during engine warm-up. The nature and topography of the impacted surfaces play an important role since while the back of the inlet valves is rather smooth, the surfaces of inlet ports are made of cast aluminum, which is quite rough. In cases where the fuel is injected directly into the cylinder, as in DI engines, the effects of droplet/wall interactions are quite evident particularly in small bore engines, where the distance between the injector and the piston head is small. Again, increased emissions of particulate matter, nitric oxides and unburned hydrocarbons have been reported (e.g., Yoshikawa, 1989; Norris-Jones et al., 1984; Matsui and Sugihara, 1988), due to spray impingement. In this context, the use of alternative fuels is pointed as a solution to decrease engine-out emissions, but again it needs to be carefully analyzed, as the different properties of these fuels are expected to modify the fluid dynamic and heat transfer mechanisms associated with secondary atomization and consequently, mixture preparation.

* Corresponding author. Tel.: +351 21 841 7875; fax: +351 21 849 6156.
E-mail address: moreira@dem.ist.utl.pt (A.L.N. Moreira).

0142-727X/$ - see front matter © 2006 Elsevier Inc. All rights reserved.
doi:10.1016/j.ijheatfluidflow.2006.10.004

Although engines operate over a wide range of in-cylinder temperature/pressure and load conditions, the complex thermo- and fluid-dynamic spray–wall interactions which occur in an engine environment are usually inferred from single droplet impingement in simplified geometries. Then the experiments are extrapolated based on dimensionless numbers characterizing the relative magnitude of the forces acting upon each droplet and estimated with the physical properties of the liquid, *e.g.*, Chandra and Avedisian (1991), Bussman et al. (2000) or Thoroddsen and Sakakibara (1998): the Reynolds number ($Re = \rho D_0 U_0/\mu$), the Weber number ($We = \rho D_0 U_0^2/\sigma_{lv}$) and the Ohnesorge number $[n \cdot (\rho(D_0\sigma_{lv}))^{1/2}]$, where ρ, σ_{lv} and μ are the density, the surface tension and dynamic viscosity of the liquid, respectively, D_0 and U_0 are the initial diameter and the impact velocity of the droplet and $n = \mu/\rho$ is the *kinematic* viscosity. However, the nature and topography of the surface alter the boundary conditions at impact and introduce additional effects which cannot be quantified in terms of the dimensionless groups, as claimed by Yarin (2006). These effects are extensively reported in the literature for impaction onto non-heated surfaces (e.g., Wu, 1992; Stow and Hadfield, 1981; Mundo et al., 1995; Range and Feuillebois, 1998; Kandlikar and Steinke, 2001; Rioboo et al., 2002).

But when the target is heated, impinging droplets exhibit dissimilar behaviours, depending on the influence of surface temperature, T_W, on the mechanism of heat transfer: *film evaporation* ($T_W \leqslant T_{sat}$, where T_{sat} is the liquid saturation temperature), *nucleate boiling* ($T_{sat} \leqslant T_W \leqslant T_{Nukiyama}$), *transition* ($T_{Nukiyama} \leqslant T_W \leqslant T_{Leidenfrost}$) and *film boiling* ($T_W \geqslant T_{Leidenfrost}$). These mechanisms are usually associated with three hydrodynamic regimes, namely: (i) the *wetting regime*, when the droplet contacts with the target surface; (ii) the *transition regime*, when the droplet contacts with the surface intermittently and (iii) the non-wetting regime, when the vapor layer generated between the droplet and the surface precludes the contact between them.

Numerous studies are reported which address the onset of disintegration of single droplets at the wetting regime (e.g., Akao et al., 1980; Araki and Moriyama, 1982; Naber and Farrel, 1993), at the *Leidenfrost* regime (e.g., Wachers and Westerling, 1966) or well above the *Leidensfrost* temperature (e.g., Karl et al., 1996), but the combined effects of heat transfer and the nature of the target surfaces are only sparsely reported, e.g. Karl and Frohn (2000) and Bernardin et al. (1997). Only recently, e.g. Cossali et al., 2005a, reported observations that liquid disintegration is altered by the imbalance between surface tension and friction forces simultaneously induced by heat transfer and surface topography. Moreover, experimental measurements of the temporal evolution of crown diameter and height, as well as of the size of ejected droplets, are required to model droplet impact (e.g., Roisman and Tropea, 2002) or even fuel mixture and combustion (e.g., Fan and Reitz, 2000; Tomoda et al., 2001), but have been sparsely reported. Exceptions are the works of Cossali et al. (2002, 2005a) and Akhtar and Yule (2001), although the latter considers the film boiling regime. Therefore, comprehensive studies are still required to devise physical models to predict the outcome of droplet impact onto heated rough surfaces. This is the objective of the experiments reported here.

In this context, the present work follows that reported by Moita and Moreira (2002) on the disintegration limits and addresses the characterization of the disintegration mechanisms from impacts onto cold and heated surfaces within the various boiling regimes. The experiments consider individual droplets impacting a number of rough targets, made of different materials, which cover surface roughness of typical piston surfaces, which was estimated based on measurements performed on real piston surfaces, using an optical profile meter. The surfaces are heated from ambient temperature up to 300 °C and the impact conditions cover a wide range of Weber (*We*), Reynolds (*Re*) and Ohnesorge (*Oh*) numbers ($8 < We < 2100$; $400 < Re < 1600$ and $1.8\text{E}{-4} < Oh < 1.0\text{E}{-1}$, respectively), comparable to those expected in IC engines. Surface *wettability* and topography, as well as liquid properties, are systematically varied and their relative importance is discussed within the different boiling regimes. The analysis addresses the morphology of disintegration and includes measurements of secondary droplet characteristics (size distribution, number and ejection angles). The emphasis is put on the effects of the nature of the surface.

2. Experimental

The experimental set-up and the working conditions considered throughout the work are described here, together with the experimental method.

2.1. Experimental set-up and working conditions

The experimental set-up has been extensively described in previous works (e.g., Moita and Moreira, 2002,b) for which only a summary is provided here. Droplets are generated at the tip of a hypodermic needle and fall by action of gravity onto the target surface. The flow rate into the needle is controlled by a syringe pump. The temporal behaviour of droplets upon impact is recorded by a high-speed camera triggered by the passage of the droplet through a laser beam hitting onto a photodiode. Several experiments were performed using different liquids, covering a wide range of droplet diameters and impact velocities (see Tables 1 and 2) and a wide range of dimensionless numbers (Weber, Reynolds and Ohnesorge numbers), comparable to those expected in IC engines (see Table 3).

Target plates are accommodated on a copper block heated by a 264W cartridge heater from ambient temperature up to 310 °C. The temperature is monitored by thermocouples (type K) and controlled by a PMA KS20-I temperature controller.

Table 1
Working conditions

Parameters	Range
Impact angle	$\phi_s = 0°$
Initial droplet diameter (D_0)	2.4 mm $< D_0 <$ 3.2 mm
Working temperatures	
Droplets	Ambient temperature
Impact surface	Ambient temperature $< T_W <$ 310 °C
Pressure	Atmospheric pressure
Impact velocity [$U_0 = f(H)$]	10 mm $< H <$ 1.9 m 0.44 m s^{-1} $< U_0 <$ 5.1 m s^{-1}
Working fluids	Water, ethanol, Diesel-oil, biodiesel

Table 2
Physical properties of the fluids used in the experiments

Liquid	Surface tension [N m^{-1}] $\times 10^3$ (20 °C)	Density [kg m^{-3}] (20 °C)	Kinematic viscosity [m^2 s^{-1}] $\times 10^6$ (20 °C)
Water	73.75	996.6	1.0
Ethanol	22.0	790	1.4
Diesel oil	30 (estimated)	836.6	4.3
Biodiesel	29.87	872	11.87

Table 3
Range of dimensionless numbers covered in the experiments

Dimensionless Numbers	Range covered in the experiments	Range for IC engines[a]
Reynolds	400–16000	170–3500
Weber	8–2100	300–55000
Ohnesorge	1.8E−4 to 1.0E−1	6.7E−2 to 1.0E−1

[a] Estimated using droplet diameters and velocities gathered from Arcoumanis and Cutter (1995), Arcoumanis et al. (1997) and Pitcher and Winklhofer (1998).

Homogeneity of the surface temperature is assured by thermal imaging analysis with an infrared thermal imaging camera (*NEC San-ei Instruments*, model TH1102). Thermal images of the target plates are post-processed with the *Remote Program TH51-708* software and converted into spatial distribution grids of temperature values, with 238×254 points resolution.

2.2. Experimental method

All quantities necessary to characterize the temporal behaviour of droplet upon impact, such as crown morphology, instantaneous droplet diameter and ejection angles are measured in pixels from the recorded images. Impact velocity, U_0 and initial droplet diameter, D_0 are measured directly from the frames recorded immediately before impact. Accuracy in the determination of D_0 is ±1.4% of droplet diameter and for U_0 the accuracy is ±0.1 m s^{-1}. Comparisons of measurements of U_0 with theoretical predictions were also performed as in Range and Feuillebois (1998) and were observed to be always smaller than 0.4 m s^{-1}.

Secondary droplet characteristics are obtained from image processing, making use of commercial software combined with routines developed to optimize edge detection, counting and size measurement of the droplets. The associated uncertainties are mainly due to the spatial and temporal resolution of the image acquisition system. The maximum temporal resolution achieved is 0.1 m s. The absolute resolution of the acquisition system and of the technique for image analysis allow detection of secondary droplets larger than 30 μm but, for a good accuracy on droplet counting, only secondary droplets with diameters larger than 60 μm were considered in the characterization of the secondary atomization. Secondary droplets for which $D_{max}/D_{min} > 2$ (where D_{max} and D_{min} are, respectively, the maximum and the minimum droplet diameter measured during the detection and measurement of each secondary droplet) were also rejected, as in Cossali et al. (2002).

Each experiment was repeated several times, at different periods of the progression of the work to assure reproducibility of the phenomena. To establish the disintegration limits, each experiment was also repeated, at least five times, considering droplets with the same initial diameter. Uncertainty of critical impact velocity to determine the disintegration limits is usually smaller than ±0.1 m s^{-1}. At impacts of biodiesel droplets onto smooth surfaces, uncertainty of the critical impact velocity could be, in some cases, larger than ±0.5 m s^{-1}, so most part of these measurements was not considered in the results.

2.3. Characterization of the target surfaces

The nature of target surfaces is associated with the *wettability*, quantified as the equilibrium contact angle, θ, and with the topography. The topography is characterized by roughness amplitude (mean roughness, R_a and mean peak-to-valley roughness, R_z) and by the fundamental wavelength, λ_R when the surface is regular.

2.3.1. Equilibrium contact angle

The equilibrium contact angle, θ, is defined by the Young equation $\sigma_{lv} \cdot \cos\theta + \sigma_{ls} = \sigma_{sv}$, where σ is the interfacial surface tension at the boundaries between liquid (l), solid (s) and vapor (v). Many researchers refer to the dynamic (advance and receding) contact angle as measured during droplet spread. However, although it may be useful to describe *spreading* (e.g., Pasandideh-Fard et al., 1996; Rioboo et al., 2002; Vignes-Adler, 2002), it is not directly related to the onset of *prompt splash*. Therefore, given that the equilibrium angle is a thermodynamic property which can be measured *a priori*, it is used here together with the topography of the targets to characterize the tertiary system liquid–surface–vapor.

Equilibrium contact angles are measured with sessile drops inside a thermostatted ambient chamber (Ramé-Hart Inc., USA, model 100-07-00) previously saturated with the liquid to be studied at a temperature of 20 ± 1 °C. The

chamber is equipped with quartz windows to avoid optical distortion. The surfaces are first washed with an EXTRAN + Water DD (distilled and de-ionized) solution and ultrasounds and afterwards are washed again with Water DD and ultrasounds for at least eight times.

After the droplet is deposited, its image is recorded by a colour video camera (JVC Colour TK-1070) mounted on a Wild M3Z microscope with a magnification of 40 times. The video signal is transmitted to an image processor – Video Pix Framegrabber (Sun Microsystems) – and digitized in 640×480 pixels images, in a 256 grey level scale. Image acquisition and analysis are performed by a Sun Sparc station IPC, using the Axisymmetric Drop Shape Analysis software (ADSA for SunOS 1.0 Applied Surface Thermodynamics Research Associates, Toronto, Canada). The variation of the contact angle with time is recorded at time intervals of 600 s. Average values are obtained from at least eight measurements. The time evolution of the average contact angles is obtained by curve fitting and the final values are determined by extrapolation. Since the outcome of droplet impact occurs in a much smaller time scale it is considered that the final value of the contact angle is determined by fitting the values obtained in the latest period of the measurement and extrapolating them for $t = 0$ s.

2.3.2. Surface topography

The topography of the target is characterized by roughness amplitude and wavelength. Two different profile meters were used, an optical and a mechanical. The optical profile meter (Surface Measuring System RM600-3D) scans surface structures between 0.01 μm and 600 μm, using a non-contact process. The mechanical profile meter (Perthometer C5D) uses a contact measuring process to characterize rough structures up to 250 μm.

The profile meter scans a sample profile of a given length, l_m and divide it in five sub-lengths, l_e. The roughness amplitude is characterized by the mean roughness, R_a and by the average peak-to-valley height, R_z. The mean roughness, R_a, calculated according to standard BS 1134, is the arithmetic mean amplitude of the roughness grooves, relatively to a reference mean-line. R_z, calculated according to standard DIN4768, is the average of single peak-to–valley heights from the five adjoining sampling lengths. The wavelength, λ_R, is estimated from the roughness profiles as the average length between roughness grooves.

Numerous measurements were performed along different directions in order to form a grid of small target areas with defined roughness characteristics. Heterogeneities in the region of droplet/surface interaction, as characterized by variations of the mean roughness, were found to be smaller than 10%. Ageing of the surfaces is controlled by repeating the contact angle and surface roughness measurements, at room temperature, at different periods during the experiments. The variations detected were not observed to alter significantly the results. As in most part of the studies reported in the literature, the contact angle was measured at ambient temperature.

Table 4
Main characteristics of the target plates, e.g. material, topography and *wettability* with water

Surface		R_a (μm ± 10%)	R_z (μm)	λ_R (μm)	θ (deg)
Glass	Smooth	≈ 0	≈ 0	≈ 0	13.2
	Random	2.0	12.0	–	90.0
	profile	2.7	18.0	–	57.9
Aluminum	Random profile	1.0	13.76	–	75.3
	Regular	15.0	115.5	210	85.0
	profile	41.7	184.0	530	101.5
		41.7	180.2	430	–
Copper	Random	0.543	6.0	–	90.8
	profile	1.3	9.0	–	96.5
		3.5	23.0	–	93.2
	Regular	16.8	80.0	210	–
	profile	46.46	169.7	530	121.5
		39.2	142.4	430	–
Stainless-steel	Random	0.524	9.0	–	93.5
	profile	1.287	14.5	–	88.0
		3.8	22.0	–	94.8
	Regular	17.1	81.5	210	–
	profile	42.0	175.3	530	–

Table 4 summarizes the characteristics of the targets used in the experiments in terms of material, topography and *wettability* with water. Complete wetting ($\theta \approx 0°$) is observed for all pairs surface-liquid (ethanol, Diesel-oil and biodiesel).

2.3.3. Wetting behaviour of the targets

Although it is not the scope of the paper to perform an extensive study on the *wettability*, it is necessary at this point to discuss the wetting behaviour of the surfaces used in the experiments, since it determines the disintegration mechanisms. Based on the contact angle, a partial wetting system is associated with $0° < \theta < 90°$, while for a partial non-wetting system $90° < \theta < 180°$ and for a complete wetting system $\theta = 0°$. But, when discussing droplet disintegration at impact, it is also necessary to evaluate weather the drop collapses as the liquid completely penetrates into the roughness grooves (homogeneous wetting) or traps air inside the grooves underneath the liquid and is suspended on the surface (heterogeneous wetting). In the latter case, the contact angle may be very large corresponding to a behaviour referred as super-hydrophobicity or super repellency.

The homogeneous wetting regime is well described by Wenzel's theory (1936) which relates the actual contact angle, θ_W, with the Young angle, θ_Y by the roughness ratio, r_W, representing the ratio of the true wetted area to the apparent area: $\cos\theta_W = r_W \cos\theta_Y$. The heterogeneous wetting regime is described by Cassie and Baxter (1944) and the apparent angle, θ_{CB} is given by: $\cos\theta_{CB} = -1 + f(r_f \cos\theta_Y + 1)$ where f is the fraction of the projected area of the solid surface wetted by the liquid and r_f is the roughness ratio of the wetted area.

Each equation predicts a quite different behaviour, e.g. Quéré et al. (2003) and each one gives a different angle at the equilibrium state of minimum Gibbs energy for the same surface which, in turn, depends on the wetting regime. The transition between the homogeneous and the heterogeneous wetting regimes is not clear, e.g. Patankar (2003) and Marmur (2003), but is known to depend on surface chemistry and roughness, e.g. He et al. (2003) and Extrand (2002, 2004).

The very rough surfaces used in the present work form a complete wetting system with fuels with small surface tension, but have high contact angles with water (see Table 4). To infer the wetting regimes and the influence of the topography on the rough target plates, an analysis is performed on the target surfaces with regular profiles, which can be approximated by grooves of thickness a spaced at a constant average wavelength, λ_R, as shown in Fig. 1.

The ratio $r_g = \left(\frac{\lambda_R}{a} - 1\right)$ together with the static contact angle was suggested by He et al. (2003) to define the condition for determining the transition between homogeneous and heterogeneous regimes. Since grooves in the present work have a pyramidal shape, a is taken as the largest dimension measured from the base. The resulting values of r_g range from 1.1 and 1.3 for surfaces with large λ_R to 1.31 and 1.42 for surfaces with smaller λ_R. According to the analysis of He et al. (2003), this range of r_g, together with the contact angles measured, is associated with the homogeneous wetting regime given by Wenzel's equation.

Moreover, Bico et al. (1999) observed that the system may move from a heterogeneous to a homogeneous wetting regime if an energy barrier is transposed, for example, when the droplet is physically squeezed or falls from a certain height. He et al. (2003) observed that surfaces with this range of r_g, which are on the homogeneous wetting regime, stay in the wetting regime when the droplet falls from some height. Therefore, since the release height and impact velocities are much larger in the present investigation, the homogeneous wetting is expected to occur for all pairs liquid/regular profile surfaces. However this is only an estimative and a deeper study would require more accurate measurements and characterization of the surfaces.

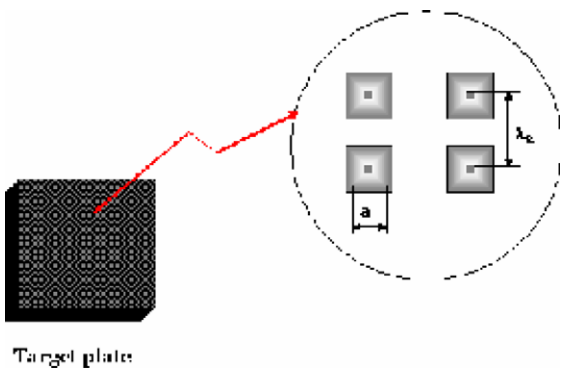

Fig. 1. Dimensions a and λ_R used to characterize roughness grooves in surfaces with regular profile.

3. Results and discussion

Disintegration of a droplet impacting onto a rigid surface occurs as the inertial effects unbalance capillary effects, i.e. as they overcome a critical value, which is commonly established as a critical impact velocity. This critical value depends on surface properties, particularly for non-heated surfaces. At surface temperatures above the ambient, heat is transferred to the impact droplet, thus altering the fluid-dynamic behaviour in a way that depends on the ratio of the time scale associated with the heat transfer to that associated with momentum transfer.

Heat transfer is usually described by the classical boiling theory, which includes film evaporation, nucleate/boiling, transition and film boiling, as depicted in Fig. 2. As the surface temperature, T_W, increases, but still below saturation ($T_W < T_{sat}$) any significant difference is observed in the disintegration mechanism or in the *splashing limits*. The time scale associated with heat transfer from the surface to the liquid is fairly small compared to the time scale associated with droplet spreading, so given that *prompt splash* mainly occurs during the initial milliseconds or even microseconds after impact, it is not much influenced by surface temperature. Major effects may be caused by continuous surface heating, which may modify surface roughness and *wettability* and decrease the critical impact velocity for *prompt splash* at rough surfaces, as reported by Bernardin and Mudawar (1996).

As the surface heats up to the liquid boiling temperature and particularly at small impact Weber numbers ($We < 100$) for which the thickness of the spreading lamella is large, the liquid film spreads and recoils as in an isothermal phase, forming a meniscus inside which vapor bubbles are formed; at larger heat transfer rates gradients of surface tension generate cellular structures (e.g., Chandra and Avedisian, 1991; Manzello and Yang, 2002); further increasing T_W up to the Nukyiama temperature causes bubbles to explode at the interface solid–liquid, from which

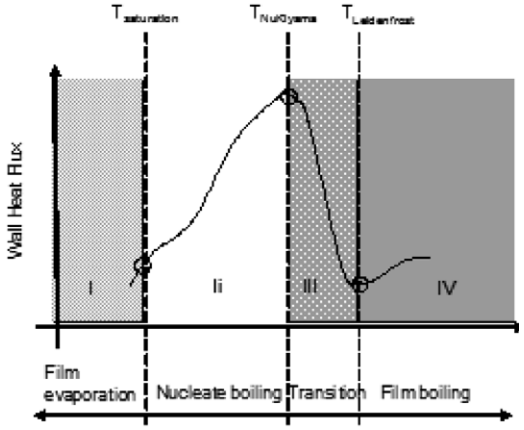

Fig. 2. Heat transfer regimes, as described by the classical boiling theory. Regimes I–IV are associated to the segments of the curve representing the wall heat flux as a function of surface temperature.

secondary droplets are ejected even at impact velocities quite bellow the critical value measured at non-heated surfaces, *e.g.* Chaves et al. (1999); as the surface approaches the Leidenfrost temperature, a vapor layer forms which applies a pressure force below the impacting droplet, precluding the contact with the surface and breaking the spreading film. At this point, droplet behaviour is significantly altered and dissimilar mechanisms occur, such as the droplet rebounds without disintegration at small Weber numbers ($We < 60$), or disintegrates a few instants after the impact at moderately high Weber numbers. Furthermore, it has been suggested that secondary droplet distribution correlates with the Weber number, e.g. Akhtar and Yule (2001).

Therefore, not only the disintegration time decreases when surface temperature increases, but also the mechanisms behind disintegration are altered. The consequence is that the same physical model cannot describe spray/wall interactions and mixture preparation in IC engines as the engine warms up after cold-start, such as in Fan and Reitz (2000) and Tomoda et al. (2001). More complex models are then required to account for the effects of surface temperature, as also suggested by Kuhnke (2004). The interactions between thermal and fluid-dynamic mechanisms also depend on the geometric boundary conditions associated with the topography of the surface and on thermodynamic conditions associated with the molecular structure of the surface and of the liquid, which have to be taken into account into these models.

This is the objective of the following analysis, where the combined effects of the heat transfer with the boundary conditions are addressed based on extensive image-based measurements. Here, the boundary conditions are described by the topography of the impacted area and by the surface Gibbs energy, as described by *wettability*. The experiments are reported under four headings, depending on the heat transfer mechanism.

3.1. Non-heated surfaces

3.1.1. The onset of splash

The most relevant fluid-dynamic mechanisms of droplet–wall interaction in IC engines are *stick–spread* and *disintegration*. Particularly, it is important to be able to predict the limiting conditions at which impacting fuel droplets stick and spread, thus contributing to the formation of unburned liquid film, or *disintegrates* into smaller droplets, contributing to ameliorate fuel vaporization and mixing. The onset of disintegration is usually described by the Weber number ($We = \rho D_0 U_0^2/\sigma_{lv}$) as in Moita and Moreira (2002). This is because disintegration results from a competition between the destabilizing kinetic energy of the droplet at impact and the stabilizing surface energy required to keep the shape of the droplet. In fact, reminding that the kinetic, E_{Ki} and the surface energy, E_{Si} of a droplet are given by $E_{Ki} = \rho U_0^2 \pi D_0^3/12$ and $E_{Si} = \sigma_{lv}\pi D_0^2$, respectively, one obtains $We = 12E_{Ki}/E_{Si}$.

Water is usually taken as a reference fluid, for which Fig. 3 depicts the critical Weber number for the onset of *splash* of water droplets as a function of surface mean roughness made dimensionless with the initial droplet radius (R_a/R_0). For ease of analysis, the data measured in the present work are plotted together with those reported by Stow and Hadfield (1981) and Range and Feuillebois (1998).

Different curves are obtained by fitting the experimental data with the correlation proposed by Wu (1992) for the critical Weber number: $We_c = a\ln^b(R_0/R_a)$, where a and b are fitting constants, which depend on the material of the target and on the liquid. The figure shows a clear dependence of the disintegration limits on the pair liquid-surface and different curves are obtained for different materials, as in Range and Feuillebois (1998) due to *wettability* effects.

The results agree with those of Stow and Hadfield (1981) and Range and Feuillebois (1998) and small deviations are attributed to different roughness profiles and materials.

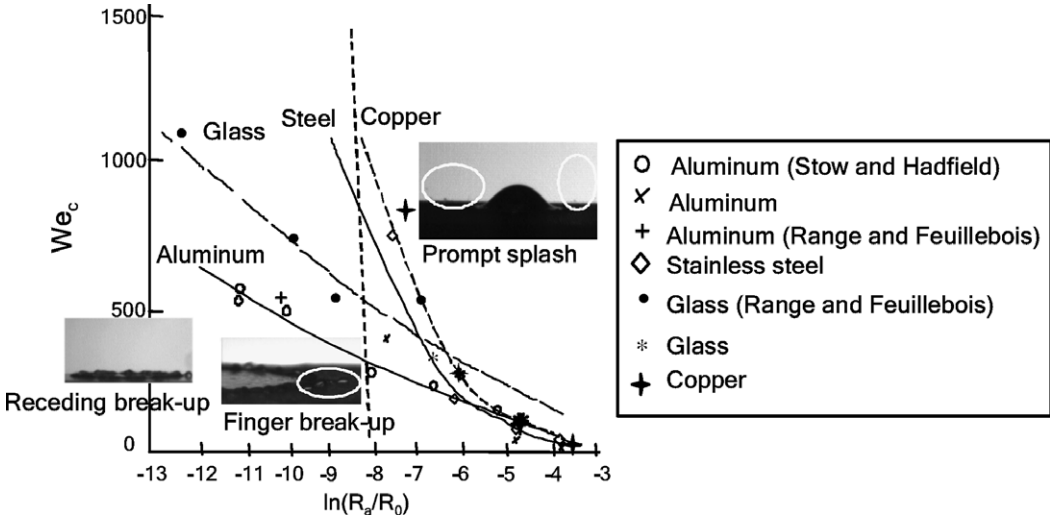

Fig. 3. Critical Weber number for disintegration of water droplets impacting onto different surfaces, as a function of dimensionless roughness.

Surface roughness endorses fast disintegration making it to occur at smaller critical velocities. However, visualization at impact morphology reveals that the effect is brought upon by different mechanisms for small and large amplitude roughness grooves, as shown in the images depicted in Fig. 3:

(i) Droplets impacting onto rough surfaces ($R_a/R_0 > 2.5E{-}3$) disintegrate by the mechanism of *prompt splash*, regardless the liquid and the surface, as the curves corresponding to the different pairs liquid/surface lean to collapse into a single curve, function of R_a/R_0. Given that wetting is expected to be homogeneous for all surfaces used in the current experiments, disintegration is attributed to the decreased thickness of the spreading lamella as it transposes a rough peak, rather than to the imbalance between inertial and surface tension forces, as in the heterogeneous wetting regime.

(ii) Droplets impacting onto smooth surfaces, $R_a/R_0 < 3.4E{-}4$, initially adhere to the surface, spread and generate fingers which grow ahead from the contact line. These fingers break-up, either due to capillary effects at later stages of spread, or during recoil if the surface energy is not enough to keep cohesion of the receding fingers when transposing surface roughness grooves. Both mechanisms were observed onto stainless-steel, copper and Perspex surfaces. Despite Range and Feuillebois (1998) report that water droplets impacting onto glass surfaces of the same dimensionless roughness ($R_a/R_0 < 3.4E{-}4$) disintegrate by *prompt splash*, this could not be confirmed in the present work as our glass target plates have different roughness characteristics.

(iii) At surfaces with intermediate roughness, $3.4E{-}4 < R_a/R_0 < 2.5E{-}3$, the three mechanisms occur simultaneously.

Although not represented in Fig. 3, the effect of increasing the amplitude of surface peaks is similar to the effect of decreasing the wavelength of peaks in regular surfaces: *prompt splash* is promoted at small impact velocities.

Liquid fuels behave differently, since they completely wet the surfaces used in the current experiments, as it happens with liquids with small surface tension. The resulting differences for water can be discussed based on the disintegration limits of ethanol, Diesel-oil and biodiesel droplets depicted in Fig. 4. It is observed that, while *prompt splash* is still the mechanism of disintegration at very rough surfaces ($R_a/R_0 > 2.5E{-}3$) and again the several curves lean to collapse into a single curve, function of R_a/R_0, Diesel-oil and ethanol droplets impacting onto surfaces with intermediate roughness ($2.0E-6 < R_a/R_0 < 2.4E{-}3$) disintegrate after *crown* formation. Surface tension of these liquids differ by only about 25% while kinematic viscosity has a ninefold increase from ethanol to biodiesel and, therefore, differences in Fig. 4 may be mainly attributed to viscosity. The results in the Figure are in accordance with the observations reported by Rioboo et al. (2000) for smooth surfaces in the sense that the threshold for the onset of *splash* increases with viscosity.

On the other hand, fuel and water droplets disintegrate by completely different mechanisms, as a clear indication of the role of the *wettability* of the system on droplet disintegration. For the complete wetting systems formed by fuel droplets ($\theta \approx 0°$), the droplet spreads and forms a crown because the restraining pressure of air creates a vertical momentum which deflects the spreading liquid upwards, by a mechanism similar to that described by Blake (1993) and Xu et al. (2005). Also, Fig. 4 clearly shows the important role of viscosity in dissipating part of the energy available for the formation of a crown, which is to be contrasted to observations in wetted and very smooth surfaces that crown formation and propagation are dominated by liquid inertia, e.g. Yarin (2006). The relative importance of

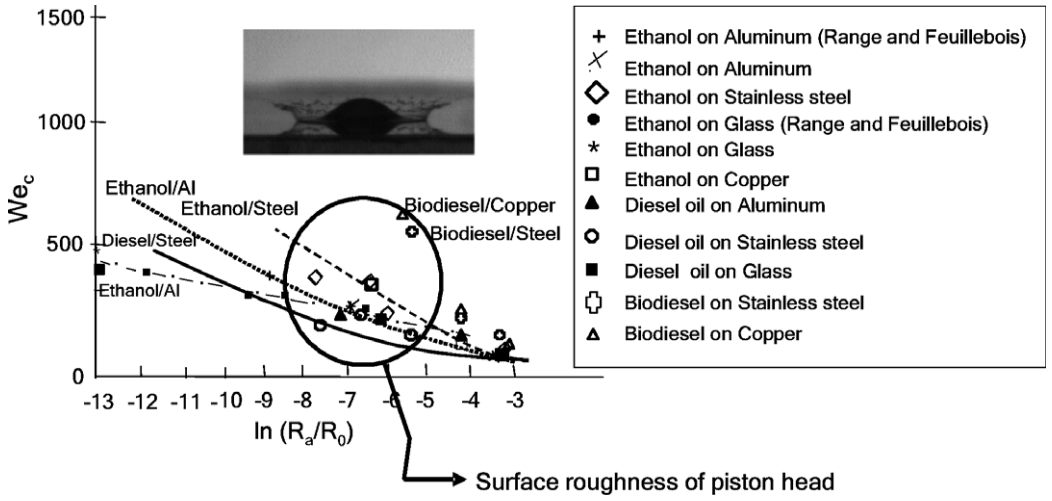

Fig. 4. Critical Weber number for disintegration of ethanol, Diesel-oil and biodiesel droplets impacting onto different surfaces, as a function of dimensionless roughness.

viscosity decreases as surface roughness increases at the same time that crown becomes less clear suggesting the contribution of roughness grooves to film destabilization.

Given the importance of a better understanding of crown formation and destabilization to accurately predict the outcome of droplet impact, a detailed analysis of the morphology of the crown is reported in the following paragraphs. The analysis considers the use of smooth aluminum and stainless-steel surfaces, for which the morphology and crown formation are similar. Also, stainless-steel and aluminum were used as an approach to applications regarding internal combustion engines.

3.1.2. Crown morphology

The foregoing discussion showed that complete crown formation occurs at very smooth surfaces which allow fast and regular spread of the lamella, since very small roughness grooves of the surface would be enough to destabilize the liquid film. Any substantial change is observed in the morphology of the crown and in secondary atomization onto rougher surfaces except for an anticipation of crown destabilization and disintegration.

Fig. 5a and b depict the temporal evolution of ethanol and Diesel-oil droplets, respectively, impinging on an aluminum surface, at nearly similar conditions. The ethanol droplet, which has a smaller surface tension and viscosity, is completed disintegrated at about 1.0 ms, when multiple jets are still observed at the crown of the Diesel-oil droplet, which extend up to until $t = 1.5$ ms and can be as long as 1.7 mm.

The dynamics of the crown can be quantified by the time variation of its geometry, making use of the lower and the upper diameters, D_l, and D_u, respectively, and crown height, H_c, as represented in Fig. 6 (e.g., Cossali et al., 2004).

These quantities are represented in Figs. 7 and 8. Fig. 7 shows that the temporal evolution of D_l and D_u for Diesel-oil and ethanol droplets impacting onto an aluminum surface have similar values which can be described by a dimensionless relation similar to that proposed by Yarin and Weiss (1995):

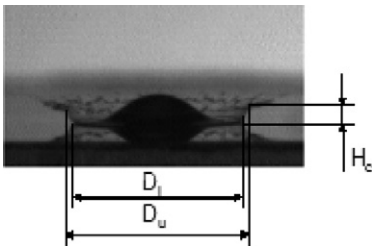

Fig. 6. Crown morphology of a *splashing* droplet: D_l – crown lower external diameter; D_u – crown upper external diameter; H_c – crown height.

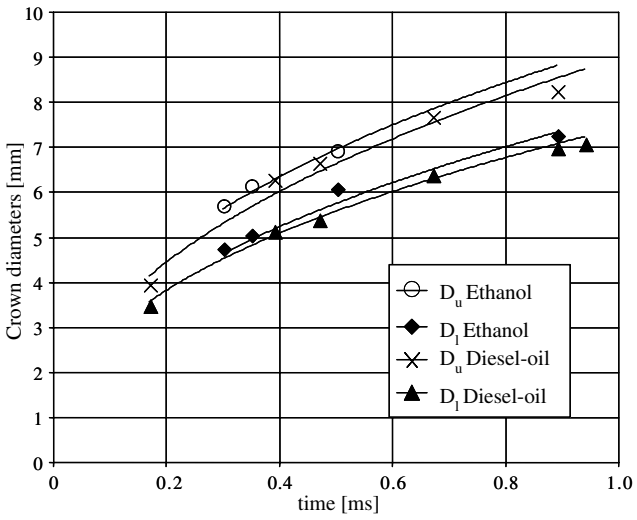

Fig. 7. Temporal evolution of crown upper and lower diameters (D_u and D_l) for ethanol ($D_0 = 2.4$ mm, $U_0 = 3.1$ m s^{-1}) and Diesel-oil ($D_0 = 2.6$ mm, $U_0 = 3.1$ m s^{-1}) droplets impacting onto an aluminum surface ($R_a = 1.0$ μm, $R_z = 13.76$ μm) at ambient temperature.

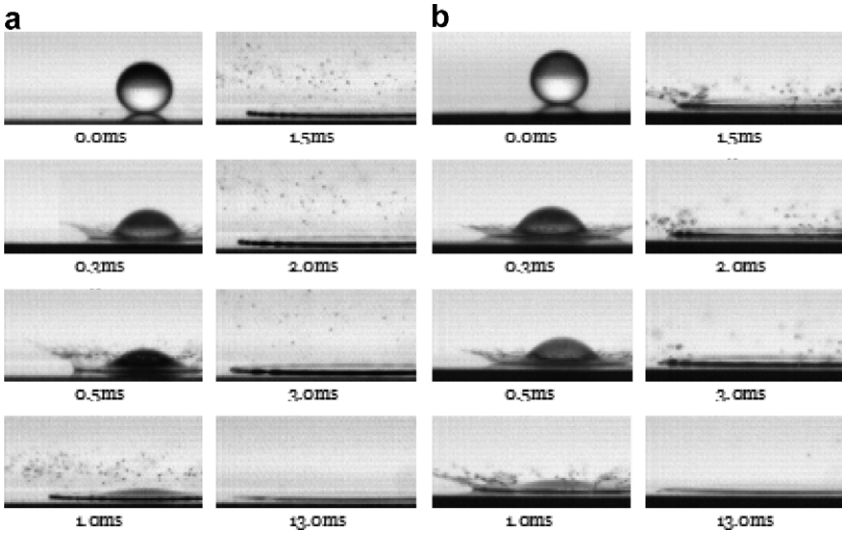

Fig. 5. Temporal evolution of *corona splash* of: (a) an ethanol droplet ($D_0 = 2.4$ mm, $U_0 = 3.1$ m s^{-1}) and (b) a Diesel-oil droplet ($D_0 = 2.6$ mm, $U_0 = 3.1$ m s^{-1}) after impacting onto an aluminum surface ($R_a = 1.0$ μm, $R_z = 13.76$ μm) at ambient temperature.

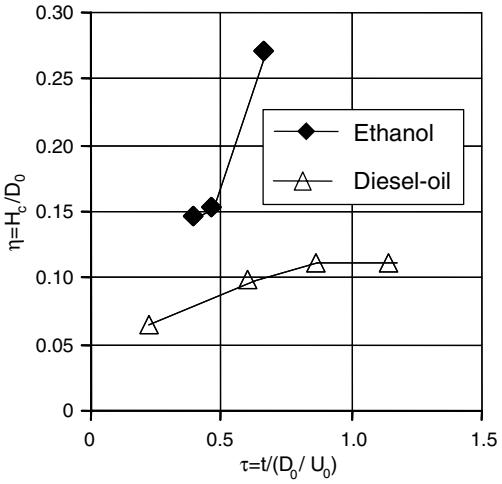

Fig. 8. Temporal evolution of dimensionless crown height, $\eta = H_c/D_0$, for ethanol ($D_0 = 2.4$ mm, $U_0 = 3.1$ m s^{-1}) and Diesel-oil ($D_0 = 2.6$ mm, $U_0 = 3.1$ m s^{-1}) droplets impacting onto an aluminum surface ($R_a = 1.0$ μm, $R_z = 13.76$ μm) at ambient temperature.

$$\frac{Dc}{D_0} = C \cdot (\tau - \tau_0)^n \tag{1}$$

where Dc is the diameter of the crown; C and n are fitting parameters. The value of C depends only weakly on liquid properties ($2.6 < C < 3.1$ and $2.8 < C < 3.4$, for ethanol and Diesel-oil, respectively) and n assumes values between 0.41 and 0.45, which are close to the value $n = 0.5$ reported in Yarin and Weiss (1995) for droplets spreading on a liquid film.

The temporal evolution of the dimensionless crown height, $\eta = H_C/D_0$ is plotted in Fig. 8. Crown height of ethanol droplets is larger and the lamella quickly destabilizes and disintegrates completely, while the jets at the crown of Diesel-oil droplets still propagate mainly in a radial direction, consistently with the large and fast increase of crown upper diameter.

Comparison of the present results with existing theoretical models would be worth at this point, but most of the research works in this field report on crown formation at wetted surfaces (e.g., Roisman and Tropea, 2002; Fedorchenko and Wang, 2004). Fig. 9 compares the results obtained here for Weber numbers ranging from 670 to 793, with those reported by Cossali et al. (2004) for droplets impacting onto liquid films at similar Weber numbers ($We = 667$ and $We = 843$) and shows that the time for crown formation and disintegration is significantly larger on the wetted surface. Although the plot depicts only the advancing phase up to $\tau = t/(D_0/U_0) = 5$, the crown on the wetted surface advances and recedes for a quite long period of time, up to $\tau = 30$. For impacts onto dry surfaces, the crown grows at a fast rate and disintegrates right after impact, at $\tau = 1$ and the height of the crown is significantly smaller. Therefore, though it is not surprising that the theoretical predictions of Roisman and Tropea (2002) agree with the experimental data reported by Cossali et al. (2004) they are not expected to fit the results reported here where the morphology of the crown is different. These differences should be considered when modeling the disintegration mechanism, since they also affect secondary droplet distributions, which are usually derived from relations based on crown diameters and height evolution.

3.1.3. Secondary droplet characteristics

In agreement with the morphological study, the most obvious factor influencing the secondary atomization is the increase of liquid viscosity, which prevails over the effects of surface topography and *wettability*. Fig. 10, represents the temporal evolution of the number of secondary droplets and of the arithmetic, D_{10}, and Sauter, D_{32}, mean diameters. The figure shows that fuels with larger viscosity produce less and larger secondary droplets, which is associated with a thicker spreading lamella. For less viscous liquids, the size distribution of secondary droplets size seems

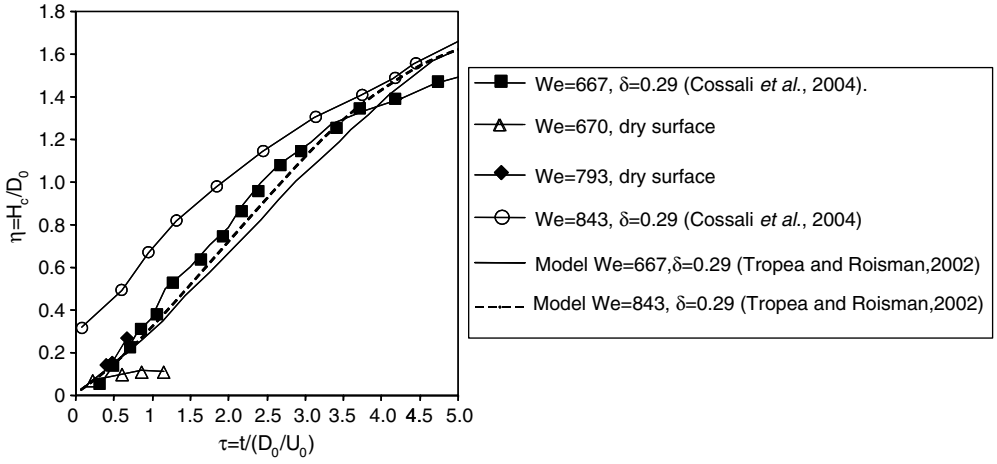

Fig. 9. Comparison of crown evolution generated from drop impacts ($670 < We < 843$) onto a dry surface (present study) and onto a wetted surface (Cossali et al., 2004). Lines represent the theoretical prediction from Roisman and Tropea (2002).

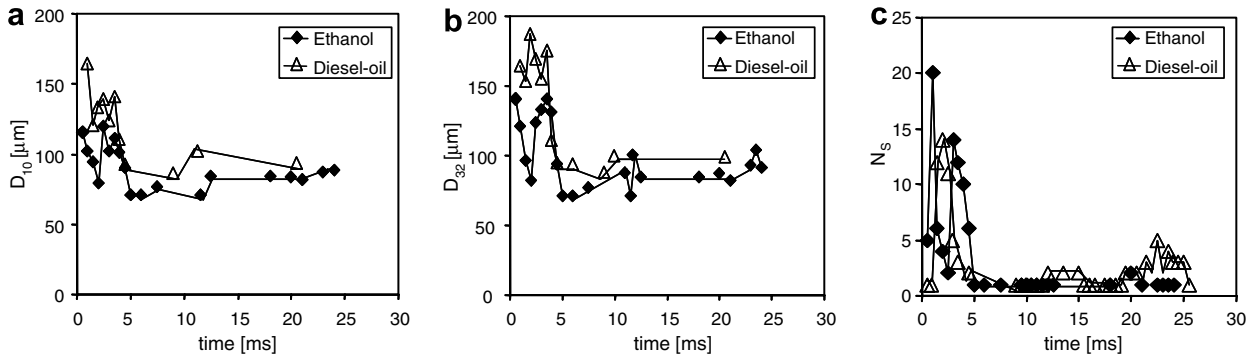

Fig. 10. Temporal evolution of (a) D_{10}, (b) D_{32} and (c) Number of secondary validated droplets, N_s, for ethanol and Diesel-oil droplets impacting onto an aluminum surface ($R_a = 1.0$ μm, $R_z = 13.76$ μm) at ambient temperature.

to be less uniform and the number of droplets is generally larger along time. The maximum value of N_s occurs at the initial instants after impact, when the rate of development of the crown is larger. The large values of mean diameters observed, however, may be partially due to the limitation of the image acquisition system, which can detect but not measure accurately droplet sizes smaller than 60 μm.

Crown angle $\gamma_c = \arctan[H_c/(D_u - D_l)]$, as estimated from crown diameter and height is shown in Fig. 11 to be larger for ethanol which is to be contrasted with the model proposed by Fedorchenko and Wang (2004), for which the angle of the crown only depends on the dimensionless depth of the liquid film.

Up to this point, the analysis focused on droplet disintegration onto non-heated surfaces. In the following we address the combined effects of heat transfer with surface properties and liquid properties.

3.2. Heated surfaces

The experiments onto heated surfaces cover the range $30 < We < 287$, although the effects of surface topography are mainly addressed for moderately low Weber numbers ($We = 62$), to ensure that dynamic conditions do not cause disintegration at $T_W < T_{sat}$. The material of the target plates is chosen to be stainless-steel since it is less sensitive to be altered by continuous heating, contrarily to aluminum plates. Here, the study only considers pure substances for a clearer analysis and also to avoid working in the limit conditions of the rig required to achieve the high Leidenfrost temperature of Diesel-oil.

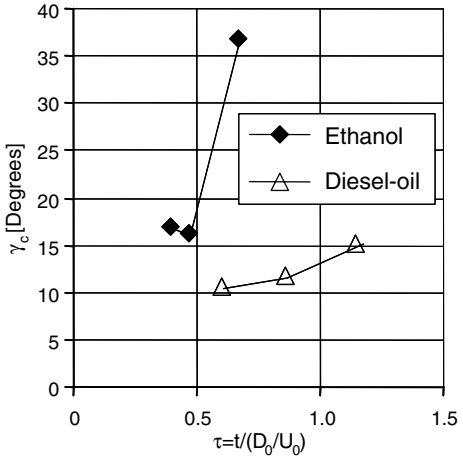

Fig. 11. Temporal evolution of crown angles for ethanol ($D_0 = 2.4$ mm, $U_0 = 3.1$ m s^{-1}) and Diesel-oil ($D_0 = 2.6$ mm, $U_0 = 3.1$ m s^{-1}) droplets impacting onto an aluminum surface ($R_a = 1.0$ μm, $R_z = 13.76$ μm) at ambient temperature.

3.2.1. Nucleate boiling regime

A slight or moderate increase of surface roughness in the nucleate boiling regime does not produce any considerable change in the morphology of disintegration and differences are only observed when the roughness is strongly increased, as depicted in Fig. 12.

The resulting effect on secondary atomization is shown in Fig. 13, which depicts the temporal evolution of the number and size of secondary droplets (N_S, D_{10} and D_{32}), generated at the impact of an ethanol droplet onto stainless-steel targets.

The figures show that secondary atomization induced by bubble explosion in a surface with mean roughness of 17.1 μm (Fig. 12b) is very intense at 5.5 ms after impact and gives rise to large secondary droplets (e.g., $t = 7.0$ ms), while for a smoother surface (Fig. 12a) disintegration begins at $t = 7.0$ ms with the ejection of numerous small droplets. This suggests that liquid boiling and bubble explosion onto rough surfaces start at earlier stages of spreading, which is attributed to the enhanced heat transfer associated with increased liquid–solid contact. Closer observation of the images (see the zoom in Fig. 14) shows that small jets also form at the top of the bubbles, which contribute to secondary atomization. Similar structures were only reported by Cossali et al. (2005a) who identified them as "pagoda-like" bubbles.

The results further show that the intense boiling induced by roughness during the initial 20 ms of spreading, significantly reduces the number of ejected droplets, but at the expense of a much larger size. This is a clear indication of the effect of roughness on the impact of droplets onto hot surfaces.

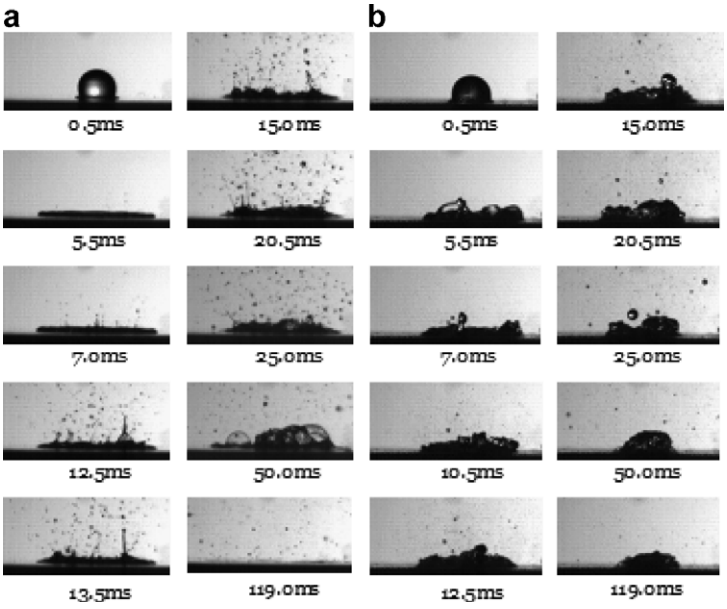

Fig. 12. Effect of surface topography on morphology of an ethanol droplet ($We = 62$) impacting on stainless-steel surfaces, within the nucleate boiling regime ($T_W = 115$ °C). (a) Smooth surface: $R_a = 0.5$ μm, $R_z = 9.0$ μm. (b) Rough surface: $R_a = 17.1$ μm, $R_z = 81.5$ μm.

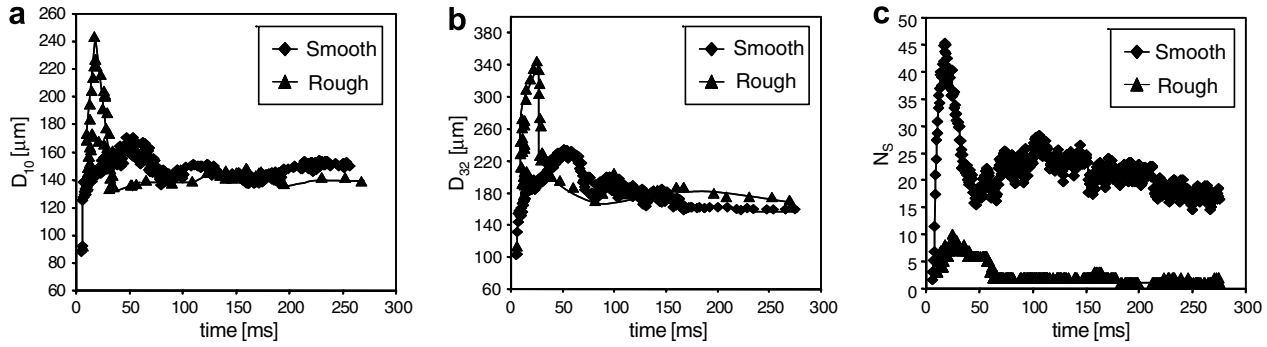

Fig. 13. Effect of surface roughness in the distributions of secondary droplets generated at impact of an ethanol droplet ($We = 62$) onto smooth ($R_a = 0.5$ μm, $R_z = 9.0$ μm) and rough ($R_a = 17.1$ μm, $R_z = 81.5$ μm) stainless-steel surfaces, within the nucleate boiling regime ($T_W = 115$ °C). Temporal evolution of: (a) D_{10}, (b) D_{32} and (c) number of secondary validated droplets, N_S.

Contrarily to observations made at cold surfaces, liquids with smaller surface tension, such as ethanol, do not form a crown at the nucleate boiling regime. However, despite the morphology of the impact is similar at high impact velocities regardless of liquid properties, differences are evident at small impact velocities for which heat transfer effects are comparatively more important. Fig. 15 illustrates the outcome of ethanol and water droplets impacting at a low Weber number onto a smooth stainless-steel surface heated at 115 °C. The differences between the two sequences of photographs are attributed to the effect of surface tension which is 3.5 times smaller for ethanol. While the ethanol droplet begins to boil at around $t = 7.0$ ms ($\tau = 3.0$), the water droplet spreads, recedes and boiling starts only at $t = 50$ ms ($\tau = 23$) after impact. Further increasing T_W up to 145 °C, near the critical flux, a fast recoil phase brings the liquid to the core region and the liquid height becomes much larger than that observed at 20.7 ms in Fig. 15b. The droplet oscillates and only at 18 ms ($\tau = 7$) after impact nucleate boiling and disintegration start.

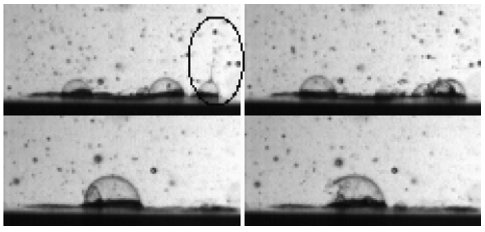

Fig. 14. "Pagoda-like" bubbles in an ethanol droplet ($We = 62$) after impacting onto a stainless-steel surface ($R_a = 0.5$ μm, $R_z = 9.0$ μm), within the nucleate boiling regime ($T_W = 115$ °C). First image highlights the ejection of the secondary droplets from the bubble.

Formation of jets such as those observed at low impact velocity onto hydrophobic surfaces, e.g. Bartolo et al. (2006) is also observed in the present work for ethanol

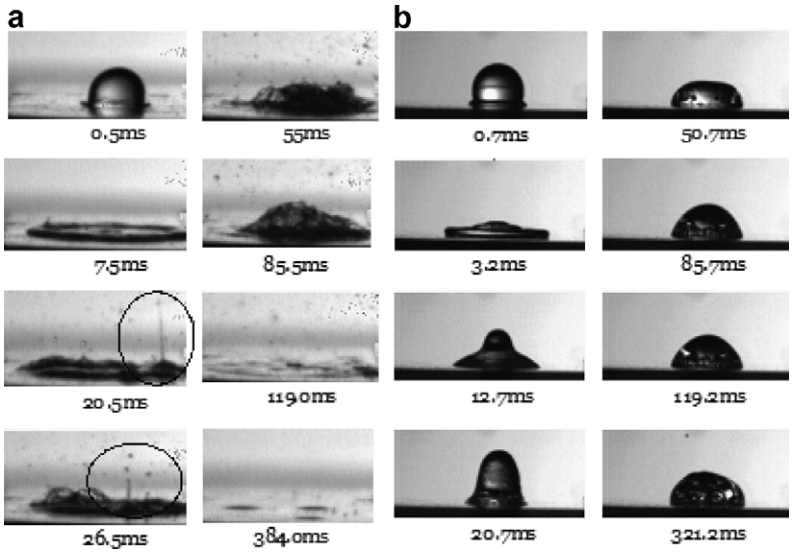

Fig. 15. Effect of liquid properties on the morphology of: (a) an ethanol droplet ($We = 62$), (b) a water droplet ($We = 60$) impacting onto a smooth stainless-steel surface ($R_a = 0.5$ μm, $R_z = 9.0$ μm), within the nucleate boiling regime.

droplets impacting onto the smooth surface, $R_a = 0.5$ μm, $R_z = 9.0$ μm, (e.g., at $t = 20.5$ ms and $t = 26.5$ ms in Fig. 15a), but is not observed at the impact of water droplets. Similar observations have been reported by Cossali et al. (2005a) at the impact of water droplets, but onto rough aluminum plates and at higher temperatures, corresponding to the film boiling regime. The fact that ethanol droplets behave similarly but in the nucleate boiling regime is attributed to the smaller surface tension which is not able to sustain vapor pressure forces. Also, the fact that this behaviour is observed to occur at the present work at a comparatively smoother surface, with which ethanol forms a completely wetting system at cold conditions, suggests that the phenomenon is not caused by entrapment of vapor within roughness grooves, as in Cossali et al. (2005a), but rather by the generation of bubbles during boiling, as described by Chaves et al. (1999).

The resulting effects on the size and number of the generated droplets is shown in Fig. 16 to be in accordance with the foregoing analysis: the larger surface tension of water keeps the liquid in the core region and decreases the contact area, thus reducing the effect of the thermal induced break-up and generating less and larger secondary droplets.

3.2.2. Transition and film boiling regimes

Fig. 17 shows sequences of images of ethanol and water droplets impacting with similar Weber numbers around $We = 280$ within the transition regime. The images were obtained at $T_W = 150$ °C for the ethanol droplet and at $T_W = 260$ °C for the water droplet. In both cases, powerful break-up of the lamella ejects droplets in the vertical direction during the initial instants following the impact, after which the remaining liquid levitates as in the film boiling regime. While this phenomenon is very clear for the water droplet at $T_W = 260$ °C (e.g., $t = 5.9$ ms), when the temperature is increased up to 300 °C, the droplet breaks-up mainly in the radial direction only after the lamella has levitated from the plate. Similar phenomena have been reported by Cossali et al. (2005b) and support that the

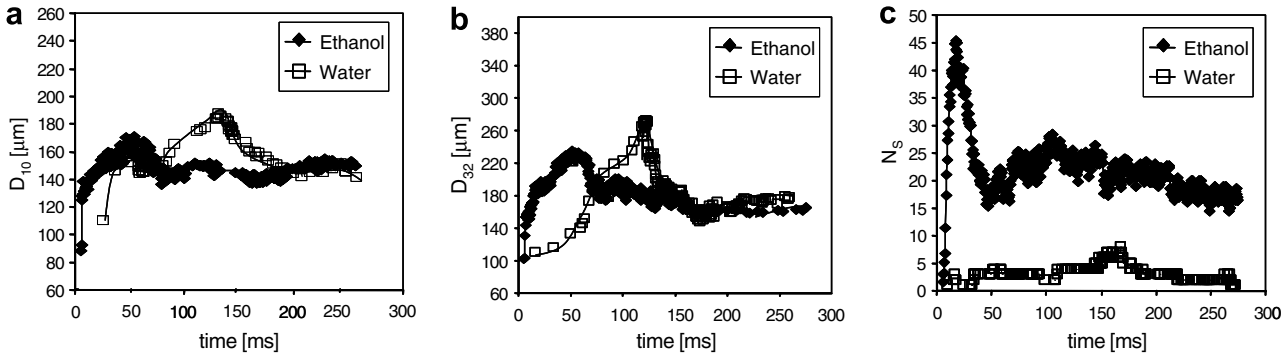

Fig. 16. Effect of liquid properties in the distributions of secondary droplets generated at the impact of ethanol and water droplets impacting onto a smooth stainless-steel surface, ($R_a = 0.5$ μm, $R_z = 9.0$ μm), within the nucleate boiling regime, at small Weber numbers ($We = 60$). Temporal evolution of: (a) D_{10}, (b) D_{32} and (c) number of secondary validated droplets, N_S.

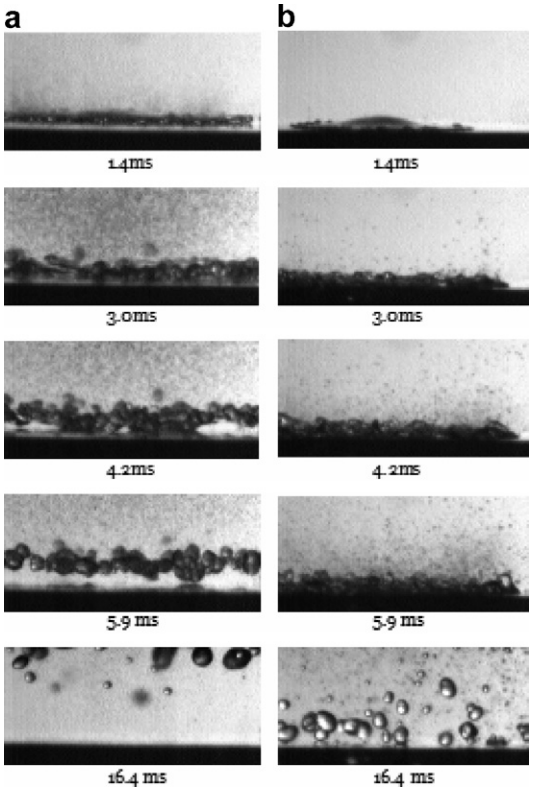

Fig. 17. Effect of liquid properties in the morphology of ethanol and water droplets impacting onto a smooth stainless-steel surface ($R_a = 0.5$ μm, $R_z = 9.0$ μm) within the transition boiling regime, at moderately high Weber numbers: (a) ethanol droplet, $We = 287$, $T_W = 150$ °C; (b) water droplet, $We = 278$, $T_W = 260$ °C.

water droplet still behaves within the transition boiling regime at $T_W = 260$ °C and film boiling only occurs at $T_W = 300$ °C.

The images then show that, within the transition regime, both liquids behave similarly and in agreement with observations reported by Cossali et al. (2005a,b), suggesting a negligible influence of surface tension at moderately high Weber numbers.

The distributions of secondary droplets generated within the transition boiling regime are depicted in Fig. 18. The results clearly show that the violent disintegration of both the water and the ethanol droplets which occurs at the initial stage of spread (e.g., $3 < t < 4.2$ ms) gives rise to a wide range of diameters. Then D_{32} increases as the secondary droplets are generated by levitation and break-up of the spreading lamella ($t = 5.9$ ms in Fig. 17). In general, the larger surface tension liquid produces less secondary droplets but with larger mean size diameters and secondary atomization starts later.

Fig. 19 illustrates the morphological behaviour of an ethanol droplet impacting onto a smooth stainless-steel surface at increasing Weber numbers, within the film boiling regime, well above the Leidenfrost temperature ($T_W > 300$ °C).

At very small Weber numbers (Fig. 19a), the droplet rebounds without break-up, as reported in several studies in the literature (e.g., Wachers and Westerling, 1966). In contrast with the lower Weber number, droplet disintegration is now clearly observed in Fig. 19b, which is associated with the increased rate of heat transfer and is an obvious effect of the increased spreading velocity of the lamella. The consequence is that the lamella stretches and thins and surface tension becomes unable to sustain vapor pressure at the solid–liquid interface. The effect of the Weber number is even clearer in the sequence of images in Fig. 19c where levitation of the lamella at the higher Weber number ($We = 278$) is observed at earlier stages of spread.

Fig. 20 points out the effects of liquid properties on droplet morphology.

The figure shows that the water droplet does not disintegrate, although may break-up during rebound, as also reported by Wachers and Westerling (1966). Actually, the droplet stretches so much as it raises from the surface that surface tension cannot keep cohesion. Conversely, the ethanol droplet breaks-up at Weber numbers only slightly larger than 60. Further increasing the Weber number the ethanol droplet breaks-up earlier and the main differences

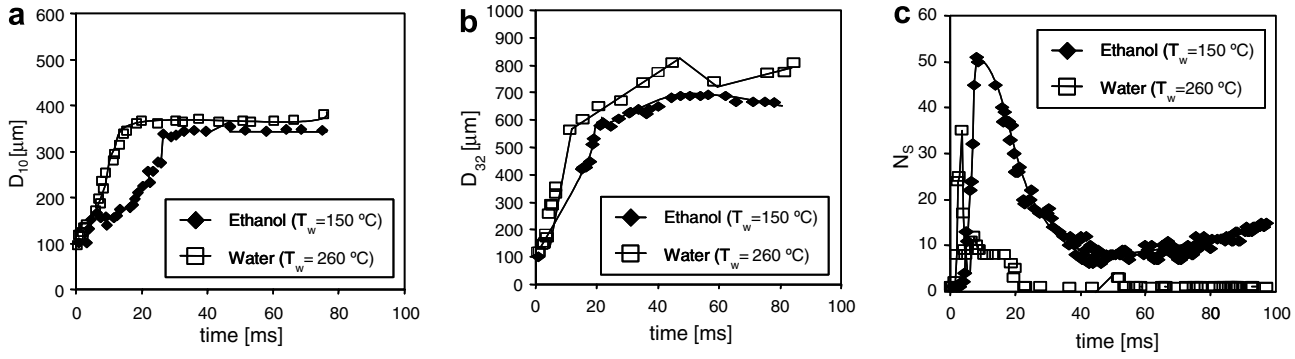

Fig. 18. Effect of liquid properties in the distributions of secondary droplets generated at the impact of ethanol and water droplets onto a smooth stainless-steel surface ($R_a = 0.5$ μm, $R_z = 9.0$ μm), within the transition boiling regime ($T_W = 150$ °C for ethanol and $T_W = 260$ °C for water) at moderately high Weber numbers ($We = 287$ for the ethanol droplet and $We = 278$ for the water droplet). Temporal evolution of: (a) D_{10}, (b) D_{32} and (c) number of secondary validated droplets, N_S.

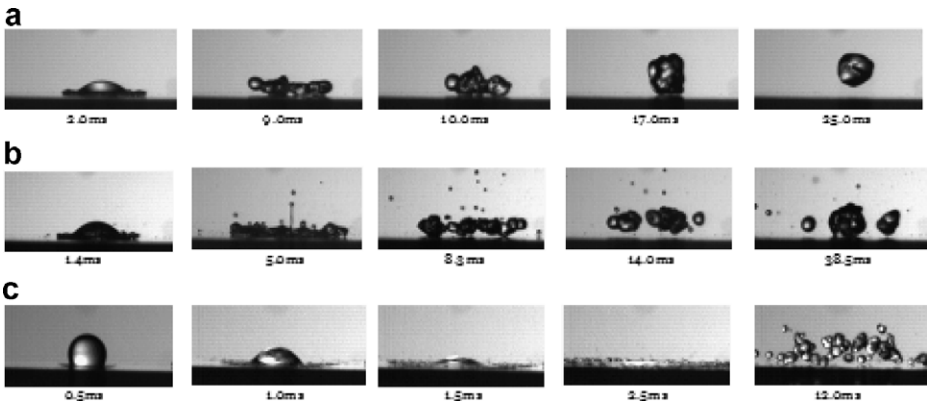

Fig. 19. Effect of the Weber number in droplet behaviour, within the film boiling regime ($T_W = 300$ °C). Ethanol droplet impacting onto a smooth stainless-steel surface, ($R_a = 0.5$ μm, $R_z = 9.0$ μm) at: (a) $We = 30$, (b) $We = 62$ and (c) $We = 287$.

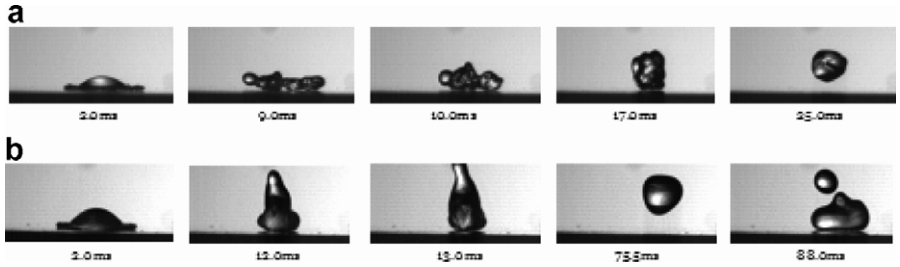

Fig. 20. Morphology of (a) an ethanol and (b) a water droplet impacting onto a smooth stainless-steel surface ($R_a = 0.5$ μm, $R_z = 9.0$ μm) within the film boiling regime ($T_W = 300$ °C), at very small Weber numbers ($We = 30$).

are observed at secondary droplet characteristics, as depicted in Fig. 21.

The figure evidences that the larger surface tension liquid gives rise to less, though larger, droplets. The overall results are in qualitative agreement with those reported by Cossali et al. (2005b): D_{32} increases at a very high rate in the range $10 < t < 20$, as in Cossali et al. (2005b). The increase of droplet diameter at $t > 40$ is not so clear with ethanol droplets, but instead droplet size tends to achieve a steady value for $t > 20$. As temperature increases up to 300 °C, the droplet reaches a stable film boiling regime and the D_{32} increases.

Fig. 22 further shows that the foregoing behaviour is altered at the rougher surface ($R_a = 17.1$ μm, $R_z = 81.5$ μm), which may be attributed to a decrease of the vapor-pressure at the interface solid–liquid as the space available within roughness grooves increases. It is such as that the liquid-surface system moves from a homogeneous wetting system at low vaporization rates to a heterogeneous wetting system at higher vaporization rates, at

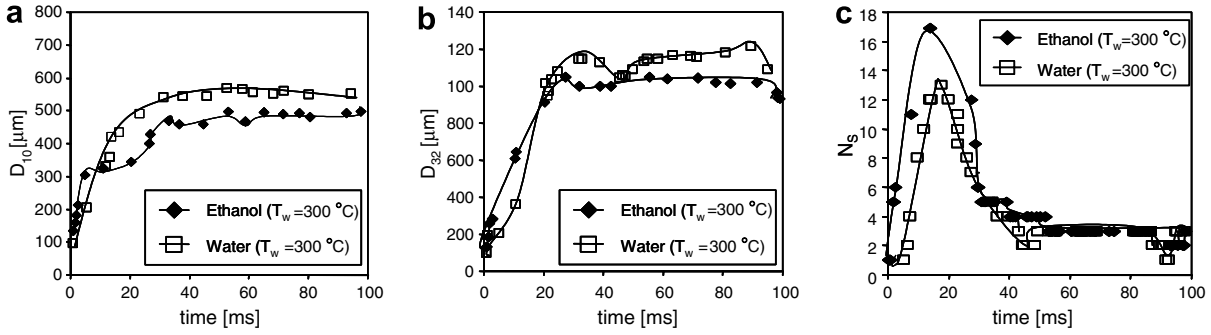

Fig. 21. Effect of liquid properties in droplet size distribution of secondary droplets generated from the impact of ethanol and water droplets impacting onto a smooth stainless-steel surface, ($R_a = 0.5$ μm, $R_z = 9.0$ μm) within the film boiling regime ($T_W = 300$ °C), at moderately high Weber numbers ($We = 287$ for the ethanol droplet and $We = 278$ for the water droplet). Temporal evolution of: (a) D_{10}, (b) D_{32} and (c) number of secondary validated droplets, N_S.

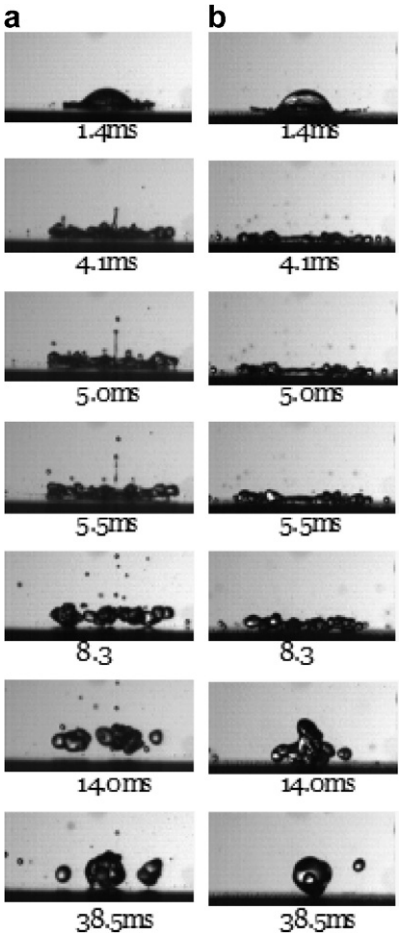

Fig. 22. Effect of surface topography on morphology of an ethanol droplet ($We = 62$) impacting on stainless-steel surfaces, within the film boiling regime ($T_W = 300$ °C): (a) smooth surface: $R_a = 0.5$ μm, $R_z = 9.0$ μm and (b) rough surface: $R_a = 17.1$ μm, $R_z = 81.5$ μm.

which the vapor pressure keeps the liquid suspended above the grooves without break-up. As a consequence, the spreading of the lamella is faster and when break-up occurs, secondary droplets are larger than onto the smooth surface, as confirmed in Fig. 23.

The effect of surface roughness in secondary droplet size is shown in Fig. 23 to be qualitatively similar to that observed within the nucleate boiling regime, in the sense that the impact onto a rough surface gives rise to less, but larger secondary droplets. Some secondary droplets generated at the first stages of spreading coalesce and give rise to very large drops with mean diameter above 1 mm.

The analysis performed so far shows that disintegration phenomena is influenced by liquid properties, surface topography and *wettabilty*, which produce different effects when combined with the heat transfer. This means that similarity rules cannot be applied and universal relations cannot be devised. However, correlations may be devised within each boiling regimes, for the number and size of secondary droplets.

Such a correlation may be obtained for the film boiling regime, as suggested by the strong effect of the Weber number in droplet morphology. Few studies reported in the literature focus on this subject. Akhtar and Yule (2001) propose a correlation for the number of secondary droplets, N_s obtained from visualization of the impaction of water droplets onto smooth stainless-steel surfaces, at Weber numbers up to 750 within the transition and film boiling regimes.

Fig. 24 depicts the results obtained in the present work together with the experimental data of Akhtar and Yule (2001), up to $We = 400$. The present data fit the correlation both within the film boiling and the transition regimes and N_s increases with the Weber number, despite N_s obtained in this study at the film boiling regime ($T_W > 300$ °C) is smaller than those reported by Akhtar and Yule (2001). It is worth noting however that the Weber number does not vary much in the present study and it was kept low to assure that it was below the critical impact conditions at $T_W < T_{sat}$, so that disintegration would be essentially thermally induced. Furthermore the correlation was developed for water droplet with $We > 100$, so it overestimates N_s obtained in the present study for water droplets at smaller Weber numbers. However it agrees well with the results obtained with ethanol, which generally disintegrates easily, according to the previous analysis.

Deviations between the experimental data presented here and the correlation by Akhtar and Yule (2001) are

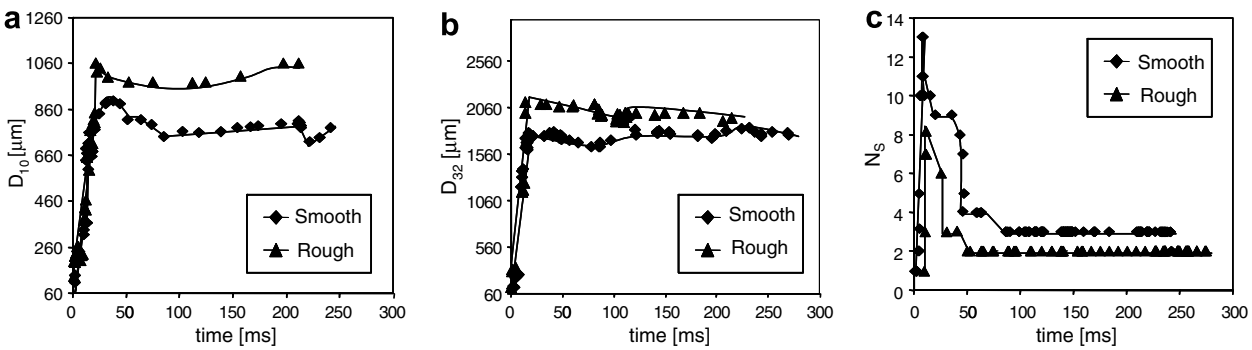

Fig. 23. Effect of surface roughness in the distributions of secondary droplets generated at the impact of an ethanol droplet ($We = 62$) onto smooth ($R_a = 0.5$ μm, $R_z = 9.0$ μm) and rough ($R_a = 17.1$ μm, $R_z = 81.5$ μm) stainless-steel surfaces within the film boiling regime ($T_W = 300$ °C). Temporal evolution of: (a) D_{10}, (b) D_{32} and (c) number of secondary validated droplets, N_S.

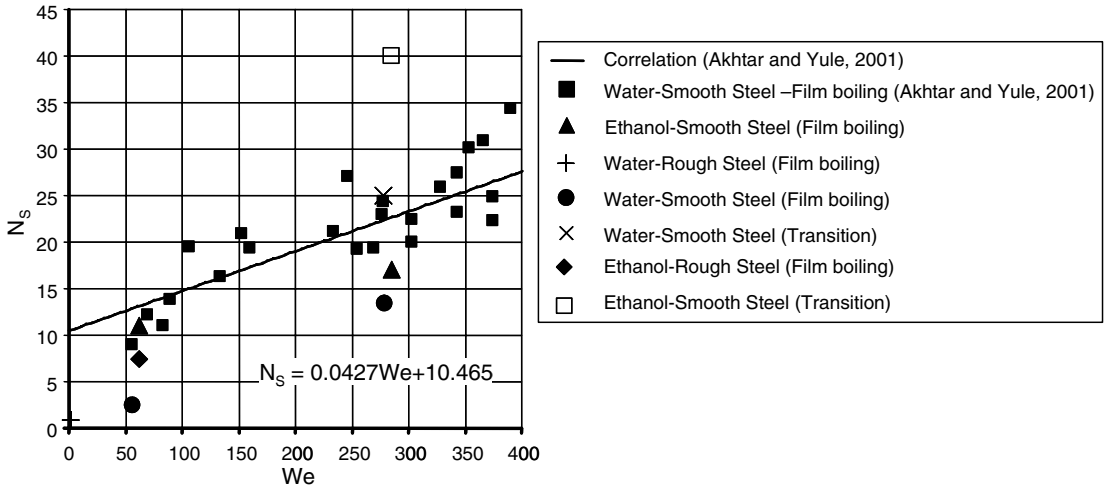

Fig. 24. Number of secondary droplets within the transition and film boiling regimes, as a function of the impact Weber number.

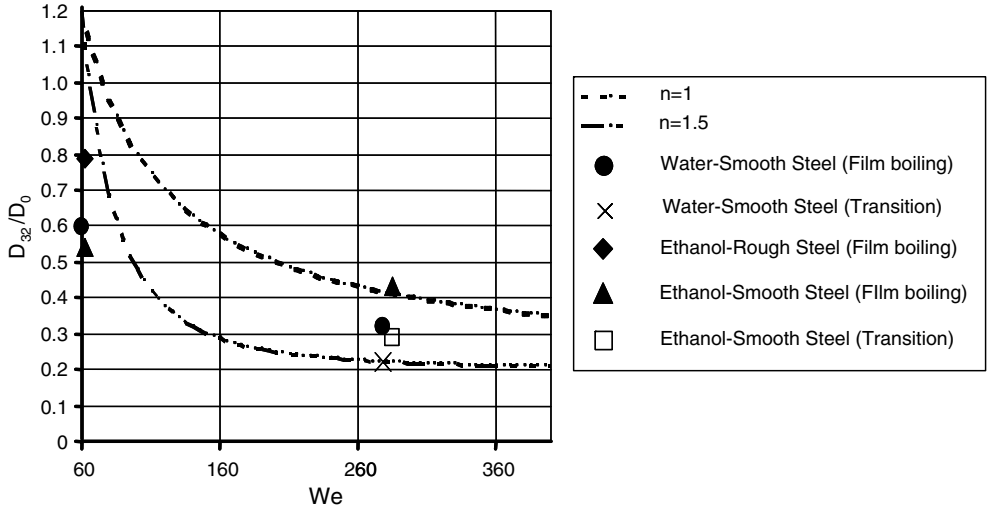

Fig. 25. Main re-atomized droplets SMD made dimensionless with D_0, within the transition and film boiling regimes, as a function of the impact Weber number.

particularly evident at impacts onto strong rough surfaces, as Akhtar and Yule (2001) did not take into account the effect of surface topography. however a further study with more experimental conditions it required to propose a correlation which accounts with this effect.

Akhtar and Yule (2001) also propose a correlation to predict the mean diameter of secondary droplets within transition and film boiling regimes:

$$\frac{D_{32}}{D_{32\text{primary droplet}}} = C + \left(\frac{60}{We}\right)^n \quad \text{with } 1.0 < N < 1.5 \qquad (2)$$

where C is a fitting constant.

Considering the time average droplet size estimated after it achieves a constant value and $D_{32\text{primary droplet}} = D_0$, the results obtained in the present investigation are shown in Fig. 25 to fall within the region defined by the correlation, but for $0.1 < n < 2.5$, for $We > 200$.

4. Conclusions

The present work addresses a fundamental study on the disintegration of fuel droplets at the impact onto cold and heated surfaces. The experiments make use of high-speed visualization together with image processing techniques to characterize the morphology of the impact and to quantify the outcome of secondary atomization in terms of droplet size and number. The analysis is aimed at evaluating the combined effects of heat transfer with the wetting behaviour of fuel droplets as it occurs in fuel injection systems of internal combustion engines.

Impacts at cold surfaces evidence a strong dependence of the morphology and limits of disintegration on surface topography and *wettability*. Although mean roughness decreases the critical velocity for disintegration, *wettability* determines the mechanism of break-up at small rough sur-

faces: receding break-up occurs at relatively high contact angle ($\theta > 90°$), while disintegration with crown formation occurs for complete wetting systems ($\theta \approx 0$).

Analysis shows that liquid fuels completely penetrate into roughness grooves of metallic surfaces and form a homogeneous wetting system, which is shown to be an important feature in shaping droplet behaviour. The most obvious consequence is that disintegration onto cold surfaces occurs with crown formation. Whereas surface roughness does not bring about important changes, increasing surface tension or viscosity increases crown growth rate, shifts the disintegration mechanisms to larger Weber critical numbers and gives rise to less and larger secondary droplets.

At the nucleate boiling regime, rupture of the spreading lamella occurs when vapor-pressure forces at the liquid–solid interface overcome surface tension forces: a large surface tension allows the liquid to keep at the core region and decreases the heat transfer area, thus reducing the effect of thermal induced break-up and generating less and larger secondary droplets; increased Weber numbers ease break-up due to the decreased thickness of the spreading lamella. Moreover, liquid boiling and bubble explosion onto rough surfaces start at early stages of spreading which is attributed to the enhanced heat transfer associated with increased liquid–solid contact. Consequently, the size of secondary droplets also increases at rougher surfaces.

The behaviour within the film boiling regime is characterized by changes in the wetting regime brought about by combined effects of heat transfer with droplet impact velocity, surface topography and liquid properties. The relative importance of the dynamic vapor pressure associated with vaporization and the spaces inside the grooves varies with the impact Weber number and plays a major role: at low Weber numbers droplets rebound before stick and surface and liquid effects are negligible; at moderately high Weber numbers the spreading lamella stretches and thins and surface tension becomes unable to keep cohesion against vapor pressure. Here, the effect of increasing surface roughness is due to an increase of the size of vapor-bubbles at the interface solid–liquid as the space available within surface grooves increases. As a consequence secondary droplets are larger than onto smoother surface. Analysis further supports a dependence of the number and size of the secondary droplets on the Weber number.

Acknowledgements

A.S. Moita acknowledges the contribution of the National Foundation of Science and Technology by supporting her with a Fellowship (Ref: SFRH/BD/18250/2004). The authors thank to Professor Rogério Colaço, from the Department of Materials Engineering of Instituto Superior Técnico, to Professor Olinda Conde, from Faculdade de Ciências da Universidade de Lisboa, to Professor Benilde Saramago and to Doctor Ana P. Serro, from the Structural Chemistry Center of Instituto Superior Técnico for providing the facilities to measure the contact angles and to characterize the roughness of the surfaces.

A.S. Moita is grateful to Professors G.E. Cossali and Marco Marengo for receiving her in a training stage and particularly to Doctor M. Santini, whose guidelines and advices were a strong help and encouragement to improve the processing procedure.

References

Akao, F., Araki, S., Mori Moriyama, A., 1980. Deformation behaviour of a liquid droplet impinging onto a hot metal surface. Trans. ISIJ 20, 737–743.

Akhtar, S.W., Yule, A.J., 2001. Droplet impaction on a heated surface at high Weber numbers. ILASS-Europe 2001, Zurich.

Araki, K., Moriyama, A., 1982. Deformation behaviour of a liquid droplet impinging on a hot metal surface. Iclass 1982, 389–396.

Arcoumanis, C., Cutter, P.A., 1995. Flow and heat transfer characteristics of impinging Diesel sprays under cross-flow conditions. SAE Paper 950448.

Arcoumanis, C., Whitelaw, D.S., Whitelaw, J.H., 1997. Gasoline injection against surfaces and films. Atomizat. Sprays 7, 437–456.

Bartolo, D., Josserand, C., Bonn, D., 2006. Singular jets and bubbles in drop impact. Phys. Rev. Lett. 96, 124501.

Bernardin, J.D., Mudawar, I., 1996. Experimental and statistical investigation of change in surface roughness associated with spray quenching. Int. J. Heat Mass Transfer 39 (10), 2023–2037.

Bernardin, J.D., Stebbins, C.J., Mudawar, I., 1997. Effects of surface roughness on water droplet impact history and heat transfer regimes. Int. J. Heat Mass Transfer 40 (1), 73–78.

Bico, J., Marzolin, C., Quéré, D., 1999. Pearl drops. Europhys. Lett. 47 (2), 220–226.

Blake, T.D., 1993. Dynamic contact angles and wetting kinetics. In: Berg. J.C. (Ed.), Wettability, p. 251.

Bussman, M., Chnadra, S., Mostaghimi, J., 2000. Modeling the splash of a droplet impacting a solid surface. Phys. Fluids 12 (12), 3121–3132.

Cassie, A.B., Baxter, S., 1944. Wettability of porous surfaces. Trans. Faraday Soc. 40, 546–551.

Chandra, S., Avedisian, C.T., 1991. On the collision of a droplet with a solid surface. Proc. R. Soc. London, Ser. A 432, 13–41.

Chaves, H., Kubitzek, A.M., Obermeier, F., 1999. Dynamic processes occurring during the spreading of thin liquid films produced by drop impact on hot walls. Int. J. Heat Fluid Flow 20, 470–476.

Cossali, G.E., Marengo, M., Santini, M., Watanabe, J., 2002. Secondary droplet atomization from single drop impact on heated surfaces. In: Proceedings of 18th ILASS-Europe2002, Zaragoza, pp. 111–116.

Cossali, G.E., Marengo, M., Coghe, A., Zhdanov, S., 2004. The role of time in single droplet splash on thin film. Exp. Fluids 36 (6), 888–900.

Cossali, G.E., Marengo, M., Santini, M., 2005a. Secondary atomization produced by single drop vertical impact onto heated surfaces. Exp. Therm. Fluid Sci. 29, 937–946.

Cossali, G.E., Marengo, M., Santini, M., 2005b. Effects of wall effusivity on secondary droplet atomization from single and multiple impact onto heated surfaces. In: Proceedings of 19th ILASS-Europe 2005, Orléans, France.

Extrand, C.W., 2002. Model for contact angles and hysteresis on rough and ultraphobic surfaces. Langmuir 18, 7991–7999.

Extrand, C.W., 2004. Criteria for ultralyphobic surfaces. Langmuir 20, 5013–5018.

Fan, L., Reitz, R.D., 2000. Spray and combustion modelling in gasoline direct-injection engines. Atomizat. Sprays 10, 219–249.

Fedorchenko, A.I., Wang, An-Bang, 2004. On some common features of drop impact on liquid surfaces. Phys. Fluids 16 (5), 1349–1365.

He, B., Neelesh Patankar, A., Lee, J., 2003. Multiple equilibrium droplet shapes and design criterions for rough hydrophobic surfaces. Langmuir 19, 4999–5003.

Kandlikar, Satish G., Steinke, Mark E., 2001. Contact angles of droplets during spread and recoil after impinging on a heated surface. J. Ch. Eng. Res. Des. 79, 491–498.

Karl, A., Frohn, A., 2000. Experimental investigation of interaction processes between droplets and hot walls. Phys. Fluids 12 (4), 785–796.

Karl, A., Anders, K., Rieber, M., Frohn, A., 1996. Deformation of liquid droplets during collisions with hot walls: experimental and numerical results. Part. Syst. Charact. 13, 186–191.

Kuhnke, D., 2004. Spray Wall Interaction Modeling by Dimensionless Data Analysis. Ph.D. Thesis, accepted by Fachbereich Mathematik, Technischen Universitat Darmstadt.

Manzello, S., Yang, J.C., 2002. An experimental study of high Weber number impact of methoxy-nonafluorobutane $C_4F_9OCH_3$ (HFE-7100) and *n*-heptane droplets on a heated solid surface. Int. J. Heat Mass Transfer 45, 3961–3971.

Marmur, A., 2003. Wetting on hydrophobic rough surfaces: to be heterogeneous or not to be. Langmuir 19, 8343–8348.

Matsui, Y., Sugihara, K., 1988. Sources of hydrocarbon emissions from a small direct injection Diesel engine. JSAE Review 7.

Moita, A.S., Moreira, A.L., 2002. The deformation of single droplets impacting onto a flat surface. SAE 2002 Trans. – J. Fuels Lubrificants, USA, 1477–1490.

Moita, A.S., Moreira, A.L., 2002b. The dynamic behaviour of single droplets impacting onto a flat surface. ILASS-Europe 2002, 157–162.

Mundo, C.H.R., Sommerfeld, M., Tropea, C., 1995. Droplet–wall collisions: experimental studies of the deformation and break-up processes. Int. J. Multiphase Flow 21 (2), 151–173.

Naber, J.D., Farrel, P., 1993. Hydrodynamics of droplet impingement on a heated surface. SAE Paper 930919.

Norris-Jones, S.R., Hollis, T., Waterhouse, C.N.F., 1984. A study of the formation of particulates in the cylinder of a direct injection Diesel engine. SAE Paper 840419.

Pasandideh-Fard, M., Quiao, Y.M., Chandra, S., Mostaghimi, J., 1996. Capillary effects during droplet impact on a solid surface. Phys. Fluids 8 (3), 650–658.

Patankar, N.A., 2003. On the modeling of hydrophobic contact angles on rough surfaces. Langmuir 19, 1249–1253.

Pitcher, G., Winklhofer, E., 1998. Droplet size and velocity measurements in the spray of a Direct Injection Gasoline injector. ICLASS-Europe'98.

Quéré, D., Lafuma, A., Bico, J., 2003. Slippy and sticky microtextured solids. Nanotechnology 14, 1109–1112.

Range, Kai, Feuillebois, François, 1998. Influence of surface roughness on liquid drop impact. J. Col. Int. Sci. 203, 16–30.

Rioboo, R., Tropea, C., Marengo, M., 2000. Outcome from a drop impact on solid surfaces. Atomizat. Sprays J. 4.

Rioboo, R., Marengo, M., Tropea, C., 2002. Time evolution of liquid drop impact onto solid, dry surfaces. Exp. Fluids 33 (1), 112–124.

Roisman, I.V., Tropea, C., 2002. Time evolution of liquid drop impact onto a wetted wall: description of crown formation and propagation. J. Fluid Mech. 472, 373–397.

Stow, C.D., Hadfield, M.G., 1981. An experimental investigation of fluid flow resulting from the impact of a water drop with an unyielding dry surface. Proc. R. Soc. London, Ser. A 373, 419–441.

Thoroddsen, S.T., Sakakibara, J., 1998. Evolution of the fingering pattern of an impacting drop. Phys. Fluids 10, 1359–1374.

Tomoda, T, Kubota, M, Shimizu, R., Nomura, Y., 2001. Numerical analysis of mixture formation of a direct injection gasoline engine. In: The Fifth International Symposium on Diagnostics and Modeling of Combustion in Internal Combustion Engines, Comodia 2001, Nagoya.

Vignes-Adler, M., 2002. Physico-chemical aspects of forced wetting. In: Rein, Martin (Ed.), Drop–Surface Interactions. SpringerWien, New-York, p. 103.

Wachers, L.H.J., Westerling, N.A.J., 1966. The heat transfer from horizontal plate to sessile water drops in the spheroidal state. Chem. Eng. Sci. 21, 923–936.

Wenzel, R.N., 1936. Resistance of solid surfaces to wetting by water. Ind. Eng. Chem. 28 (8), 988–994.

Wu, Z., 1992. Modélisation et calcul implicite multidomaine d'écoulements diphasiques gas-gouttelettes. Ph.D. Thesis, Université Pierre et Marie Curie, Paris, France.

Xu, L., Zahang, W.W., Nagel, S.R., 2005. Drop splashing onto a dry smooth surface. Phys. Rev. Lett. 94, 184505.

Yarin, A.L., 2006. Drop Impact Dynamics: Splashing, Spreading, Receding, Bouncing …. Annu. Rev. Fluid. Mech. 38, 159–192.

Yarin, A.L., Weiss, D.A., 1995. Impact of drops on solid surfaces: self-similar capillary waves and splashing as a new type of kinematic discontinuity. J. Fluid Mech. 283, 141–173.

Yoshikawa, S., Furusawa, R., Ariai, M., Hiroyasu, H., 1989. Optimizing spray behavior to improve engine performance and to reduce exhaust emissions in a small D.I. Diesel engine. SAE Paper 890463.